Fine Structure of the Main Transition in Amorphous Polymers: Entanglement Spacing and Characteristic Length of the Glass Transition. Discussion of Examples

E. Donth,* M. Beiner, S. Reissig, J. Korus, F. Garwe, S. Vieweg, S. Kahle, E. Hempel, and K. Schröter

Fachbereich Physik, Universität Halle, 06099 Halle (Saale), Germany

Received December 19, 1995; Revised Manuscript Received May 2, 1996[⊗]

ABSTRACT: The main transition of amorphous polymers is analyzed with respect to a fine structure by means of new experimental dynamic shear, dielectric, and heat capacity data for the following polymers: poly(*n*-alkyl methacrylate)s with alkyl = methyl, ethyl, propyl, butyl, and hexyl, polystyrene, poly(vinyl acetate), a series of weakly vulcanized natural rubbers, a series of butyl rubbers with different carbon black content, polyisobutylene, and bromobutyl rubber. The components of the fine structure are assumed to be a proper glass transition at short times, followed by a confined flow zone, and, at large times, a hindering zone caused by entanglements at large times. Two lengths are assumed to correspond to the first and third components, respectively, the characteristic length to the proper glass transition and the entanglement spacing to the hindering zone. The confined flow will be described by a dispersion law (general scaling) across the main transition. The characteristic length of the glass transition for the poly(*n*-alkyl methacrylate)s—only of order 1 nm as determined by calorimetry—is confirmed by backscaling from the entanglement spacing by means of a Rouse dispersion law for shear. The fate of the Rouse modes below the $\alpha\beta$ splitting of the glass transition is discussed for the other amorphous polymers. Finally, a speculative molecular picture of the different modes in the main transition is described. The new element is a low-viscosity longitudinal motion of individual chain parts in the confined flow zone. A simple rheological model for the confined flow is also presented.

I. Introduction

There is a growing evidence that the main transition of amorphous polymers, i.e. the transition from the glassy zone at higher frequencies ω to the rubbery plateau zone at lower frequencies,[1] is a thermorheologically complex phenomenon. In comparison to the glass transition (α) in small-molecule systems, different modes of molecular motion can be identified (an extensive review is given by Ngai and Plazek[2]). An alternative term for this phenomenon is fine structure of the main transition.[3]

To be precise, in our terminology the main transition is *formally* divided into three log ω ranges that are called zones (Figure 1). Different names for the zones are listed in Table 1. Our terminology of the succeeding zones is also presented in ref 4.

In the glassy zone the shear storage modulus G_g' is of order gigapascal for both polymers and small-molecule glass formers. We therefore expect that the first zone, the "proper" glass transition, can be identified in the case of fine structure components at the high-frequency side of the main transition.

The length scale of the glass transition is hotly debated,[5−9] but there is growing evidence[10−15] that the length ξ_α (of order 3 nm) estimated from the fluctuation formula[16,17]

$$\xi_\alpha^{\,3} \approx kT_g^{\,2}\Delta c_p/\bar{c}_p^{\,2}\rho\delta T^2 \qquad (1.1)$$

is reasonable for the size of molecular cooperativity (Δc_p is the step height of the specific heat capacity $\bar{c}_p$ at the glass temperature T_g, δT^2 is the temperature fluctuation of the natural functional α subsystem,[16] as estimated from the width of the transformation interval,[18,19] and ρ is the density).

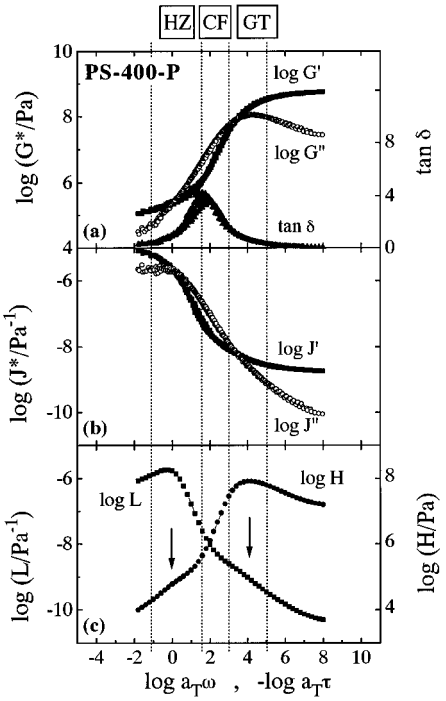

Figure 1. Master plot of (a) shear modulus, G^*, and mechanical loss tangent, tan δ, (b) shear compliance, J^*, and (c) retardation spectrum, L, and relaxation spectrum, H, for polystyrene (PS-400-P). The reference temperature is 117.6 °C. The postulated fine structure of the main transition with the three components hindering zone (HZ), confined flow (CF), and proper glass transition (GT) is indicated. Slight shoulders in the L and H spectra were observed at the same frequency position as the main peak in the complementary spectrum (see arrows).[42] The log symbols in this paper always mean $\log_{10}$.

An inspection of shear curves in ordinary amorphous polymers such as poly(vinyl acetate) (PVAC)[20] or poly-

* E-mail: donth@physik.uni-halle.d400.de.

[⊗] Abstract published in *Advance ACS Abstracts,* August 15, 1996.

S0024-9297(95)01881-X CCC: $12.00

Table 1. Different Names for the Three Zones of the Main Transition

	zone 1 high frequency	zone 2 middle part	zone 3 low frequency
log ω range in Figure 1	5−3	3.0−1.2	+1.2 to −1.1
Ngai, Plazek, et al.	local segmental	sub-Rouse	(modified) Rouse
Donth et al.	proper glass transition	confined flow	hindering zone
acronyms used here	(P)GT, α	CF	Hz

Table 2. Exponents of the Four Shear Functions and Maximal Loss Factor (tan δ) for the Rouse Model, for the Rouse−Zimm Model, for the Middle Part (CF; See Figure 1 and Table 1) of the Experimental Main Transition in Two Typical Amorphous Polymers, and for Newtonian Flow ($G^* = G' + iG''$, Shear Modulus; $J^* = J' - iJ''$, Shear Compliance)

substance/model	d log G'/d log ω	d log G''/d log ω	d log J'/d log ω	d log J''/d log ω	tan δ (max)
Rouse	0.5	0.5	−0.5	−0.5	1.0
Rouse−Zimm	0.67	0.67	−0.67	−0.67	1.73
PS-400-P (this work)	1.12	0.87	−0.28...−1.1[a]	−0.87	3.5−4.2
PVAC (Plazek[20])	1.45	0.90	−0.14...−1.3[a]	−0.91	ca. 5.7
Newtonian flow (Maxwell element)	2	1	0	−1	$1/\omega\tau_0$

[a] Changing from ... to ...; see Figure 1.

styrene (PS) shows that the middle part of the main transition (second zone) cannot generally be described by Rouse or Rouse−Zimm modes (see Figure 1 and Table 2).

The figures in Table 2 show that the middle part of the main transition can rather be described as a kind of flow similar to small-molecule systems. Assuming formally a viscosity η_{CF} for the "confined flow zone" (CF),[16,21] it must be small as compared to the viscosity η_0 of the flow zone beyond the terminal dispersion. Thus η_{CF} is of order $G_g'\tau_\alpha \ll \eta_0$, with τ_α the characteristic relaxation time for the α relaxation.

For longer times the chain connectivity of the monomeric units hinders and finally stops the flow by the entanglement.

Let us first discuss this phenomenon for the case of Rouse modes[22] at temperatures above the $\alpha\beta$ splitting region (β is a local process). It is experimentally verified there by dynamic neutron scattering[23,24] that larger modes are connected with larger relaxation times,

$$\lambda_p^4 \sim \tau_p \tag{1.2}$$

Such a relation between relaxation time τ_p of mode number p and extent of motion λ_p will be called a "dispersion law" or a general scaling law.[16] The term dispersion law in this context must be clearly distinguished from the analogous term in condensed matter physics where it describes the relation between wavelength and frequency of phonons in crystalline matter. The dispersion law for a flow process is naively expected to be similar to hydrodynamic or diffusion modes,

$$\lambda^2 \sim \tau \tag{1.3}$$

Alternative models are described in refs 25 and 26.

At large lengths and correspondingly long times, the Rouse modes are hindered by a process with a characteristic length scale[27] that is usually identified with the entanglement spacing d_E[28] of order 3−10 nm,

$$d_E = aZ_e^{1/2} \tag{1.4}$$

where a is the Ferry structure length (usually $a \approx 0.7$ nm for vinyl polymers) and Z_e is the degree of polymerization corresponding to an entanglement molecular mass M_e. The latter can be estimated from

$$M_e = \rho RT/G_N^0 \tag{1.5}$$

where G_N^0 is the shear plateau modulus.[1]

Coming back to the flow, we assume similarly that the longer and slower flow modes are hindered and finally stopped by the entanglements. In other words, the flow is spatially confined by the entanglements, and the corresponding dispersion zone is called the hindering zone (HZ).

Let us recall that the entanglement spacing has two different aspects with regard to the following plateau zone. It stops the shorter modes at its short-time end (hindering zone), and it defines the geometric scale for tying and loosening the entanglements themselves at its long-time end (flow transition), e.g. by a reptation process.

Taking ξ_α for the lower bound and d_E for the upper bound of the spatial range for the main transition modes, the relaxation times increase by one or two decades between $\xi_\alpha = 3$ nm and $d_E \approx 7$ nm.

Since the existence of Rouse modes as a part of the main transition is not obvious, as mentioned above, we have to ask why the Rouse type motion is absent in the main transition far below the $\alpha\beta$ splitting, or, alternatively, why the Rouse modes are "covered" by, or modified by some combination with, neighbored modes. This problem will be called "fate of the Rouse modes" when the sample is cooled below the $\alpha\beta$ splitting.

Having different zones, the degree of their mutual independence is of importance. The temperature dependence of the relaxation times in zones 1 and 3 is described by WLF-type equations.[29] The question raised above is intensified by the experimental finding[20,30] that the Vogel temperature (T_∞) for the slower zone (zone 3) is *smaller* than those of the faster one (zone 1),

$$T_{\infty 3} < T_{\infty 1} \tag{1.6}$$

This means that there is an encroachment[2] of the zones when the temperature is lowered. This implies thermorheological complexity and should be observed in practical master-curve constructions. An indication for this complexity is the "divergence"[2] or scatter (variation) in the loss factor (tan δ) curve in Figure 1. Encroachment can be discussed in terms of Ngai's coupling model.[2] An alternative theoretical explanation of eq 1.6 with the aid of preaveraging of Goldstein's energy landscape is given in ref 16.

It is an important question if the presumed dispersion law is common for the different activities or susceptibilities, such as shear G^*, J^*, dielectric ϵ^*, heat capacity spectroscopy (HCS) c_p^*, and other responses. The term common will be understood in the following sense. It is well known that all the different activities follow the

Table 3. Parameters of the Rouse−Zimm Range in the Dynamic Shear Compliance $J^*(\omega) = J'(\omega) - iJ''(\omega)$ for Five Poly(*n*-alkyl methacrylate)s[a]

	d/dec	− d log *J*″/ d log *ω*	− d log *J*′/ d log *ω*	m	G_N^0/MPa	d_E/nm	$\xi_\alpha^R(d_E)$/nm	ξ_α(DSC)/nm	T_g/°C
PMMA[b]	2.35	0.70	0.75	0.66	1.00	4.1	1.1	1.4	94 ± 2
PEMA	2.6	0.68	0.74	0.66	0.40	6.0	1.34	1.5	71 ± 2
PnPrMA[c]	2.8	0.60	0.62	0.60				1.2	46 ± 2
PnBMA	3.0	0.65	0.71	0.63	0.26	6.1	1.08	1.1	26 ± 2
PnHMA	3.0	0.67	0.74	0.65	0.135	7.2	1.28	0.8	1 ± 2

[a] *d* is the logarithmic frequency broadness, *m* is "the slope" from the maximal loss factor, $\tan\delta = J''/J' = \tan(\pi m/2)$, d_E is the entanglement spacing calculated from eqs 1.4 and 1.5 with $a = 0.7$ nm, G_N^0 was estimated from plateau modulus, ξ_α^R is the length calculated from d_E by backscaling with the Rouse dispersion law (cf. eq 1.2), ξ_α is the characteristic length (eq 1.1) from DSC,[52] and T_g is the DSC glass transition temperature. The estimated ξ_α(DSC) uncertainty is ±20%. [b] Containing obviously some plasticizer. [c] Bimodal MW distribution, so that backscaling has no sense here.

general trend *along* WLF curves when the temperature is changed. Their location *across* the main transition, however, is different,[31−38] and some hints to a general sequence are observed for different polymers.[39] The question is whether the underlying frequency scale corresponds to a common length scale, independent of the activity, or not. If we assume that the positive is true, we have an additional length label at the frequency scale: Besides the entanglement distance d_E from shear, the length ξ_α calculated from the caloric eq 1.1 should correspond to the peak of the imaginary part of the dynamic heat capacity, $c_p''(\omega,T)$(max). That is we shall attach ξ_α at the frequency of the c_p'' maximum.

The aim of this paper is to discuss the questions raised above with the aid of some new experimental findings (mainly from our laboratory) and a simple rheological model. The Rouse−Zimm modes observed in the $\alpha\beta$ splitting region of several poly(*n*-alkyl methacrylate)s are discussed in section 3A. Rouse modes observed in a series of weakly vulcanized natural rubbers are described in section 3B. The problem of labeling the calorimetric characteristic length ξ_α on the shear curves of three amorphous polymers (poly(vinyl acetate) (PVAC), polystyrene (PS), and a natural rubber (NR)) and the comparison with dielectric response in their main transitions are described in section 3C. The signal arrangement of different activities across the α transition in the $\alpha\beta$ splitting region of poly(*n*-butyl methacrylate) (PnBMA) is presented in section 3D. The additional shoulder in the shear spectra of polyisobutylene (PIB) and bromobutyl rubber (BIIR) is discussed in section 3E. Some cautious conclusions and a speculation about the complex nature of the main transition are given in the last section. In the Appendix a simple phenomenological model for confined flow is introduced.

II. Experimental Section

Materials. The poly(*n*-alkyl methacrylate)s (poly(ethyl (PEMA), *n*-propyl (PnPrMA), and *n*-butyl (PnBMA) methacrylate)s) were purchased from Polysciences. Experimental details are given in ref 40. The poly (*n*-hexyl methacrylate) (PnHMA) sample was kindly provided by Dr. G. Meier (Jülich) ($M_w = 1.37 \times 10^5$, $M_w/M_n = 2.45$; see also ref 41). The poly(methyl methacrylate) (PMMA) is a commercial product ($M_w = 6.6 \times 10^6$, $M_w/M_n = 1.84$). The glass transition temperatures for all poly(*n*-alkyl methacrylate)s are given in Table 3.

The natural rubber sample in section 3C is a linear polymer with $T_g = -68 \pm 1$ °C. The different natural rubber samples in section 3B are slightly vulcanized with 0.5, 1, 2, and 3 parts per hundred rubber (phr) dicumyl peroxide (DCP). These samples were kindly provided by Dr. G. Heinrich, Continental AG.

Experimental details for the poly(vinyl acetate) sample (PVAC) are given in refs 39 and 42. It was carefully dried prior to measurement (36 h at 105 °C under vacuum).

The polystyrene sample (PS-400-P) is a commercial product (Buna AG) with a broad molecular weight distribution ($M_w = (437 \pm 20) \times 10^3$, $M_w/M_n = 2.2 \pm 0.2$). It contains a small amount of plasticizer ($T_g = 92 \pm 1$ °C) which is stable during the measurements.

The polyisobutylene (PIB) was kindly provided by Prof. R. Schnabel (Halle) and was measured as received. It has a rather broad molecular weight distribution ($M_w = (1.3 \pm 0.2) \times 10^6$, $M_w/M_n = 4.7 \pm 0.5$) and a glass temperature of $T_g = -69 \pm 2$ °C.

The butyl rubber (Butyl 2-268) and bromobutyl rubber samples are commercial products. They contain 2% isoprene monomers. The butyl rubber samples are vulcanized (1.8 phr sulfur) and filled with different contents of carbon black N 339. All these samples were provided by Dr. G. Heinrich, Continental AG.

All molecular weights were estimated by gel permeation chromatography with polystyrene standards. The glass transition temperatures T_g are mean values calculated by an equal-area construction from DSC heating and cooling curves with a rate of ±10 K/min.

Experimental Setup. The dynamic shear modulus was measured in the frequency range from 10^{-3} to 100 rad s^{-1} using dynamic mechanical spectrometers RDA II and DSR from Rheometrics Scientific. The dielectric function was investigated by a Schlumberger frequency response analyzer FRA 1260 (Novocontrol) with a buffer amplifier of variable gain in a frequency interval from 10^{-2} to 10^6 Hz.

Dynamic heat capacity data were investigated by a custom-made heat capacity spectrometer (HCS) according to Birge and Nagel.[43] Experimental details will be published elsewhere.[38]

The temperature scale of all equipment was checked against each other with a precision of 0.5 K in the whole temperature range. Temperature gradients between samples and device thermometers are, if any, corrected for.[44] The temperature scale of previously published[45] shear compliance data for PnBMA was slightly corrected according to the calibration procedure used.

Procedures. For polymers with molecular weights not much exceeding the entanglement threshold, the rubbery plateau is not well developed. The modulus plateau value has been taken as the real part of the dynamic shear modulus at the point of minimum loss factor between the main and terminal transitions.[46] All shear spectra were calculated with the Weese−Honerkamp regularization program NLREG.[42,47] The master curves were calculated by a horizontal shift of the original data. The dielectric and mechanical isotherms in the splitting region of the poly(*n*-alkyl methacrylate)s were fitted by a sum of two Havriliak−Negami (HN) ($\epsilon^* = \Delta\epsilon/(1 + (i\omega/\omega_0)^\beta)^\gamma$) functions[48] or by their modulus counterpart, the MHN ($G^* = \Delta G/(1 + (-i\omega_0/\omega)^\beta)^\gamma$) function.[49] All ξ_α values were calculated from eq 1.1. The δT values were taken from the DSC transformation interval ΔT_h[19,50] of the heating runs divided by 2.5 for correction of structural relaxation or from HCS without correction.

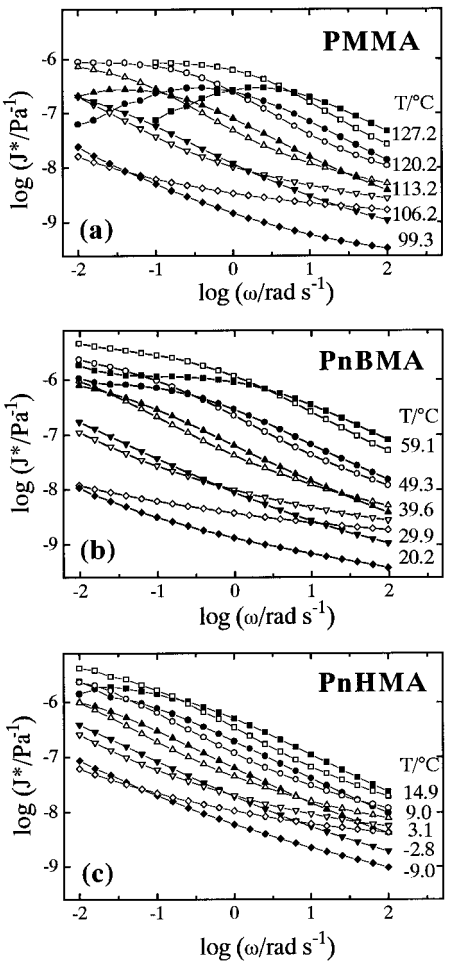

Figure 2. Real (open symbols) and imaginary parts (full symbols) of the dynamic shear compliance $J^* = J' - iJ''$ in the Rouse−Zimm part of the main transition for (a) PMMA, (b) PnBMA, and (c) PnHMA.

III. Results and Discussion

This section presents the results of several examples and discusses them with respect to length scales of the fine structure suggested.

A. Rouse Modes in Poly(*n*-alkyl methacrylate)s. As mentioned above, Rouse modes can be identified at high temperatures and frequencies, well above the $\alpha\beta$ splitting. (The latter is usually between MHz and GHz.) In poly(*n*-alkyl methacrylate)s, however, the $\alpha\beta$ splitting is systematically shifted to lower frequencies by internal plasticization due to the alkyl side groups, more than one frequency decade per additional CH_2 group,[51] so that the $\alpha\beta$ splitting can mechanically be observed in the Hz range for the butyl member, PnBMA.[50] We can, therefore, ask if the Rouse or Rouse−Zimm modes do occur in the $\alpha\beta$ splitting region and what are their changes in a "CH_2 sweep". Figure 2 shows the real and imaginary parts of the dynamic shear compliance for PMMA, PnBMA,[45] and PnHMA. All polymers show a logarithmically broad $J'-J''$ parallelism with shear exponents similar to Rouse−Zimm behavior (see Table 3). The logarithmic breadth (d) was taken as the distance between the two intersections of the J' and J'' curves (frequencies ω_E and ω_α; $d = \log(\omega_\alpha/\omega_E)$). Assuming that the α cooperativity is small (small ξ_α's) in the $\alpha\beta$ splitting, we can suppose that the Rouse−Zimm behavior is not too much disturbed.

The low-frequency intersection (ω_E) is at the J level of about 1/MPa, and the high-frequency intersection (ω_α) at about $1/10^8$ Pa^{-1}. They correspond in a way to the ends of the main transition zone and were connected with the two length labels d_E and ξ_α, respectively. The characteristic length, ξ_α^R, for the high-frequency intersection can then be backscaled from d_E by using the Rouse dispersion law, eq 1.2, and the breadth d,

$$(d_E/\xi_\alpha^R)^4 = (\omega_\alpha/\omega_E) = 10^d \qquad (3.1)$$

The results for ξ_α^R are compared in Table 3 with the characteristic length of the proper glass transition, ξ_α, obtained from DSC experiments[52] with the aid of eq 1.1. Both lengths are of order 1 nm. This means that the calorimetric length ξ_α is supported by the Rouse scaling.

For PMMA the $\alpha\beta$ splitting is in the MHz range and we expect larger cooperativity for α in the 1 Hz region. This is indicated by larger ξ_α values for PMMA (and PEMA) and by larger shear exponents in Table 3.

B. Rouse Modes between the Entanglements of Weak NR Networks. The monomeric unit of natural rubber, polyisoprene (PI), has a dipole component along the chain, so that the low-frequency end of the entanglement plateau ("normal mode process"[53]) is dielectrically indicated.[53−55] Rescaling the Kotaka et al.[53] normal mode ϵ'' maxima with the (Gaussian) end-to-end distance of their monodisperse polyisoprene polymers, we obtain, for $T_{ref} = 0$ °C,

$$(R/\text{nm}) = 22.9(\omega/\text{rad s}^{-1})^{-0.138} \qquad (3.2)$$

(corresponding to $M_e \sim \tau^{2.7}$).

In a network the cross-link distance d_c comes into play as a new length scale. Then the low-frequency end of the main transition is also dielectrically indicated.[56,57] Figure 3 shows the shear storage modulus, G', and the dielectric loss function ϵ'' master curves for four weakly vulcanized (0.5, 1, 2, and 3 phr DCP) samples. An attempt is dared to define a Rouse region R by the shear exponent value 0.5 for d log G'/d log ω. As expected, this region is also dielectrically active.

Figure 4 shows the dielectric loss function of the four natural rubbers at 0 °C. These (and the curves at other temperatures) are analyzed *successively* by the following steps. [Only the original data in the most reliable frequency range 10^0-10^4 Hz are used for the analysis.] (1) At lower temperatures, the curves are mastered relative to the (large) α peak (indicated on the right-hand side of Figure 4 by an arrow), and after a separate α Havriliak−Negami (HN) fit a WLF curve for the α maximum frequencies was estimated. (2) Fixing these α HN parameters, an additional sum of two HN functions, one for the Rouse modes (R) and the other for network modes (N), was adjusted to the data. (3) The frequencies for the three HN ϵ'' maxima are calculated: ω_{max}^{α}, ω_{max}^{R}, and ω_{max}^{N}. Their values for $T = 0$ °C are listed in the last three columns of Table 4. (4) To reduce the number of free parameters it was further assumed that the temperature shift of all these frequencies is approximately determined by the α WLF parameters.

Table 4 shows the results of an attempt[56] to calculate characteristic lengths by using eq 3.2 as a guide line for the whole frequency region of the master curves. Three lengths are calculated: d_c from ω_{max}^{R} (third column of Table 4), ξ_α^T from ω_{max}^{α} (fourth column), and λ^N from ω_{max}^{N}. Since the exponent in eq 3.2 is small, the lengths calculated are not very sensitive to possible errors in the ω_{max} values. Additionally, the first two

Table 4. Characteristic Lengths of the NR Network Samples[a]

phr DCP	d_c/nm (G_N)	d_c/nm (NMR)	d_c/nm (ω^R_{max})	ξ^T_α/nm (ω^α_{max})	ξ_α/nm (DSC)	λ_N/nm (ω^N_{max})	ω^α_{max}/MHz 0 °C	ω^R_{max}/kHz 0 °C	ω^N_{max}/Hz 0 °C
0.5	6.9	8.7	6.1	1.8	1.7	19.5	88	15	3.3
1.0	5.9	7.8	5.4	1.9	1.8	16.7	62	34.5	10
2.0	5.2	6.5	5.0	1.95	2.0	11.0	56.5	58.5	207
3.0	4.2	5.5	4.0	2.1	1.75	8.5	33	264	1320

[a] d_c is the network spacing from the rubbery plateau shear modulus (G_N), from the NMR method, and from the dielectric Rouse (R) maximum frequency (ω^R_{max}) via eq 3.2. ξ_α is the characteristic length for the α glass transition from the dielectric α maximum frequency (ω^α_{max}) via eq 3.2 (ξ^T_α) and from DSC via eq 1.1 (ξ_α). λ_N is the typical network mode length estimated from the dielectric N maximum frequency, also via eq 3.2. The dielectric α, R, and N maxima frequencies (see Figure 4) for $T = 0$ °C are listed in the last three columns.

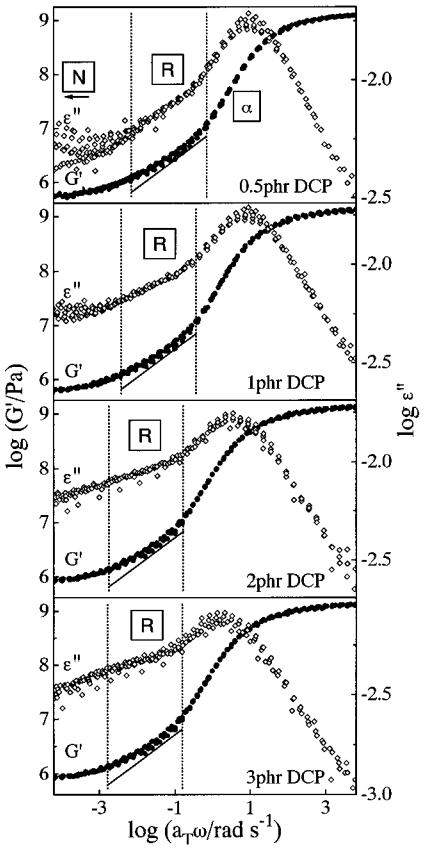

Figure 3. Master plot of the shear storage modulus, G', and the dielectric loss function, ϵ'', for four weakly vulcanized natural rubbers. The reference temperature is −60 °C. The line in the R zone indicates a 0.5 slope. The dotted lines indicate the Rouse region.

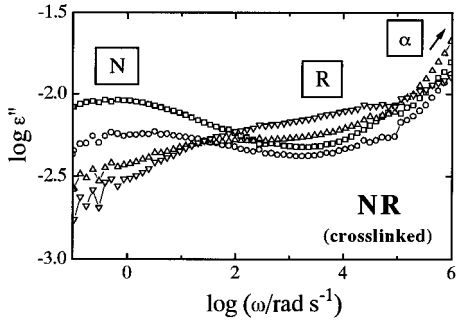

Figure 4. Dielectric loss functions for four weakly vulcanized natural rubbers at $T = 0$ °C (□) 0.5 phr DCP; (○) 1 phr DCP; (△) 2 phr DCP; (▽) 3 phr DCP). Normal modes (N), Rouse-like modes (R), and α relaxation (α) are indicated.

columns show the Cartesian distance between network links estimated by other methods. The first one is calculated from the rubber plateau modulus (G_N) using eqs 1.4 and 1.5 with G_N instead of G^0_N, and $a_{PI} = 0.7$ nm. The second one shows d_c values obtained from a NMR method.[58]

The agreement of the three values for the network length d_c is satisfying; also the trend is as expected. The characteristic lengths of the proper glass transition also fairly agree with one another.

It may be interesting that the typical length λ_N for the large network modes is steeply depressed with higher network link density, as expected from the large exponents found by Plazek for the network mode frequencies.[59]

C. Arrangement of Heat Capacity Spectroscopy (HCS) Data into the Shear and Dielectric Data of the Main Transition. Assuming a common dispersion law, we expect that the frequency of the $C_p''(\omega)$ maximum is in the proper glass transition zone. This expectation is supported by the ξ_α values obtained in the foregoing sections. The question is if the C_p'' peak is at the same frequency as the ϵ'' or the G'' peak. A coincidence of all three peak frequencies is believed by some authors[60] for small-molecule glass formers.

Figure 5 compares the $\kappa C_p''(\omega)$, $\epsilon''(\omega)$, $G''(\omega)$, and $J''(\omega)$ behavior for three amorphous polymers described in section 2: PVAC (Figure 5a),[38] PS-400-P (Figure 5b), and NR (Figure 5c).[39] Since the real part $C_p'(\omega)$ can be measured by the HCS 3ω method with much higher precision than the imaginary part $C_p''(\omega)$, the latter is calculated from HN fits of real part curves, so to speak with the aid of the Kramers−Kronig relation (for details, see ref 38).

The temperature dependences of the corresponding maximum frequencies are shown in the Arrhenius diagrams of Figure 6. As the peak maximum temperatures have an experimental uncertainty not larger than ±0.5 K (mainly from the temperature uncertainty between the samples in the different apparatus), we see from Figures 5 and 6 that the maximum frequencies of the three activities are not exactly the same: The G''_{max} frequency is significantly higher than the ϵ''_{max} frequency, whereas the C''_{pmax} frequency is in between. The sequence of the peaks is identical for all the polymers investigated here. Possible polymer-specific differences are discussed elsewhere.[61] All the three maxima are guided by (approximately parallel) WLF curves. An analysis of these curves shows[39] that the corresponding Vogel temperatures are the same (within the experimental uncertainties), but the asymptotic high-temperature WLF frequencies (order 10^{11} Hz) are different by the same amounts as indicated in Figure 6. All that means that the $C_p''(\omega)$ curves really are in the proper glass transition zone of the main transition.

We may label again this fine structure component with the characteristic length ξ_α from eq 1.1. Let us try to check the HCS ξ_α values from eq 1.1 by three different backscaling methods assuming a common

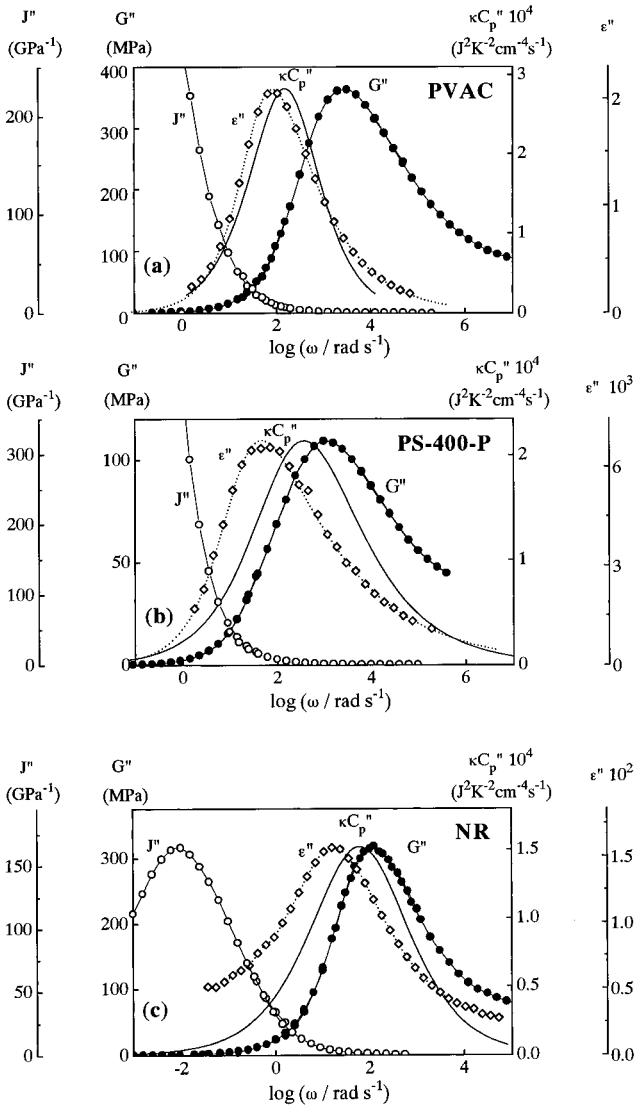

Figure 5. Frequency dependence of the dielectric loss, ϵ'' (◇), the shear loss modulus, G'' (●), the shear loss compliance, J'' (○), and the imaginary part of the entropy compliance, $\kappa C_p''$ (−), for (a) PVAC at 56.6 °C, (b) PS-400-P at 106.8 °C, and (c) natural rubber at −58.5 °C. The ϵ'' data are slightly (<0.5 dec) shifted from the experiment temperature to the common reference according to the corresponding WLF equations. The $\kappa C_p''$ curves are obtained from a HN fit to the real part $\kappa C_p'$ data (κ = heat conductivity). The J'' and G'' isotherms are master curves at the given reference temperature.

dispersion law. We start with a Rouse backscaling eq 1.2 from d_E values as calculated from eqs 1.4 and 1.5 although a Rouse region is not indicated by the shear curves. The method is demonstrated in Figure 7 for the PVAC example. The d_E value is attached to the bend frequency ω_E of $G'(\omega)$ via a tangent construction between the plateau zone and the confined flow zone. The ω_α frequency is attached to the $C_p''(\omega)$ maximum frequency. From Rouse scaling, eqs 1.2 and 3.1, $\xi_\alpha^R(d_E)$ is then obtained from

$$\xi_\alpha^R(d_E) = d_E(\omega_E/\omega_\alpha)^{1/4} \qquad (3.3)$$

The results are listed in Table 5. Although the same order of magnitude as the HCS-value ξ_α is always obtained, satisfying agreement between ξ_α and $\xi_\alpha^R(d_E)$ is only obtained for the PS sample. Saving the general idea, we can say that we have no sure knowledge about the underlying dispersion law of the confined flow zone

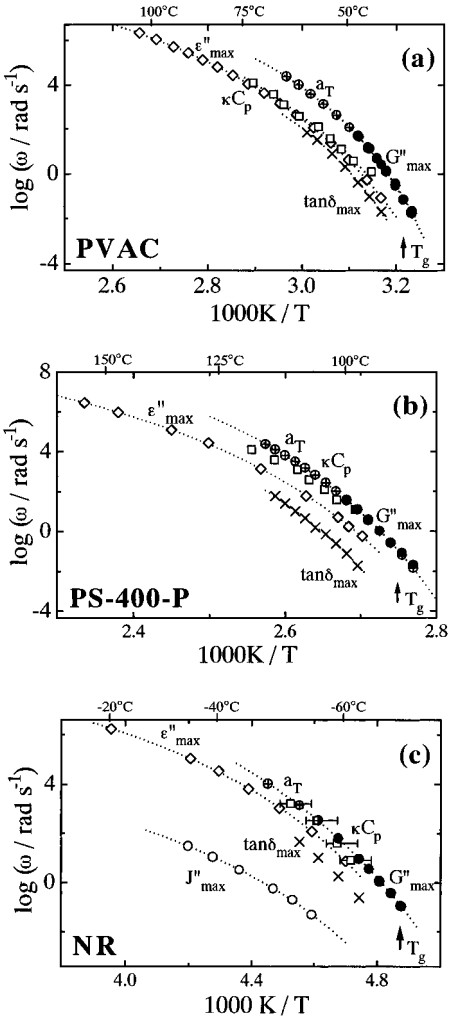

Figure 6. Temperature dependence of the main transition for (a) PVAC, (b) PS-400-P, and (c) NR. The α traces for the maxima in dielectric loss, ϵ''_{max} (◇), shear loss modulus, G''_{max} (●), shear loss compliance, J''_{max} (○), mechanical loss factor, tan δ_{max} (×), and the frequency temperature position of half step height in entropy compliance $\kappa C_p'$ (□) are shown. Additionally, the shift factors a_T (⊕) from a master curve construction for G^* are presented. The drawn curves are fits of the WLF equation. The DSC glass transition temperatures ($\dot{T}$ = 10 K/min) are indicated by arrows. The extraordinary large temperature uncertainty of the $\kappa C_p'$ measurement for NR is indicated by error bars.

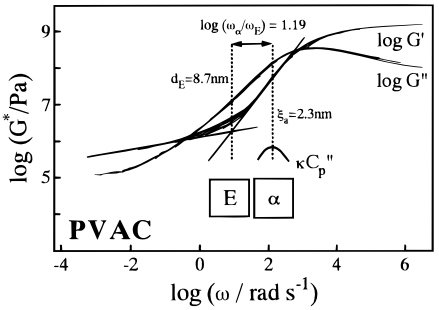

Figure 7. Master plot of the shear modulus (G',G'') and scheme for backscaling in the main transition for PVAC (T_{ref} = 56.6 °C). The corresponding $\kappa C_p''$ isotherm is also indicated. The frequency position of the entanglement spacing d_E at the onset of the entanglement plateau and of the characteristic length ξ_α at the α maximum in $\kappa C_p''(\omega)$ are indicated by dotted lines.

for larger shear exponents, much larger than 0.5 or 0.67. (The d log G'/d log ω values of Table 5 are also larger than the d log G'/d log ω value of the vulcanized NR

Table 5. Entanglement Spacing (d_E), Ferry Structure Length (a), Characteristic Length of the Proper Glass Transition Zone ξ_α from Backscaling Using the Scaling Law of Hydrodynamic Modes ($\xi_\alpha^H(d_E)$), Rouse Modes ($\xi_\alpha^R(d_E)$), and the Normal Mode (Eq 3.2, $\xi_\alpha^T(d_E)$) and, for Comparison, from DSC by Eq 1.1, and the Largest Shear Exponent, d log G'/d log ω

	d_E/nm	a/nm	$\xi_\alpha^H(d_E)$/nm	$\xi_\alpha^R(d_E)$/nm	$\xi_\alpha^T(d_E)$/nm	ξ_α(HCS)/nm	d log G'/d log ω
PVAC	8.7	0.70	2.2 ± 0.4	4.4 ± 0.4	6.0 ± 0.5	2.3 ± 0.4	1.23
PS	9.6	0.75	0.4 ± 0.1	2.0 ± 0.3	4.1 ± 0.4	1.8 ± 0.4	1.12
NR	4.5	0.70	$0.3^{+0.1}_{-0.2}$	$1.0^{+0.3}_{-0.4}$	$2.0^{+0.3}_{-0.5}$	2.4 ± 0.4	0.97

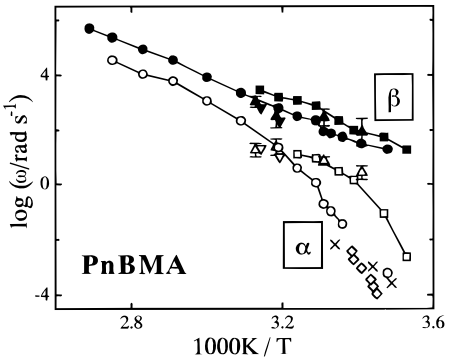

Figure 8. Arrhenius plot for the $\alpha\beta$ splitting region of PnBMA. The α (open symbols) and β peak maximum positions (full symbols) for the different activities are shown: (○,●) dielectric function;[62] (□,■) shear modulus;[51] (▽,▼) photon correlation spectroscopy, data taken from retardation spectra;[65] (△,▲) 2D-NMR relaxation time;[63] (×) entropy compliance, taken from MDSC measurements;[64] (◇) entropy compliance, frequency calculated according to eq 3.5 from DSC measurements with different heating rate, log $a = -1$.

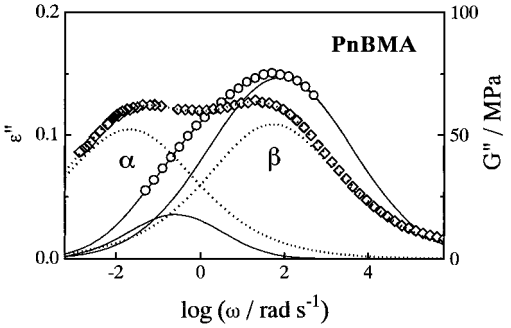

Figure 9. Dielectric loss, ϵ'' (◇), and shear loss modulus, G″ (○), versus log ω at $T = 22$ °C for PnBMA. The dotted (for ϵ'') or solid (for G'') lines are fits to the data by a superposition of two HN ($\epsilon^* = \Delta\epsilon/(1 + (i\omega/\omega_0)^\beta)^\gamma$) or MHN ($G^* = \Delta G/(1 + (-i\omega_0/\omega)^\beta)^\gamma$) functions.

samples of section 3B, the latter was about 0.8 as can be seen in Figure 3). Moreover, the attaching of ω_E to the tangent construction of Figure 7 could also be questioned.

Using alternatively hydrodynamic scaling via eq 1.3, i.e.

$$\xi_\alpha^H(d_E) = d_E(\omega_E/\omega_\alpha)^{1/2} \tag{3.4}$$

smaller ξ_α values are obtained (Table 5) than from eq 3.3. From the normal mode dispersion law eq 3.2, however, larger values ($\xi_\alpha^T(d_E)$) result. A comparison of the different characteristic lengths ξ_α with ξ_α (HCS) in Table 5 suggests that a smaller dispersion law exponent is needed for coincidence at larger shear exponents.

D. Different Activities in the Splitting Region of PnBMA. It may be an interesting question if a signal arrangement across the glass transition, similar to the polymers of Figure 6, can also be observed in the $\alpha\beta$ splitting region of PnBMA, where the α cooperativity sets in.[50,62]

The Arrhenius diagram of the $\alpha\beta$ splitting region in PnBMA is shown in Figure 8. This diagram is similar to the one published in ref 63 (containing the G'' peaks, the ϵ'' peaks, and the two relaxation times obtained from two-dimensional exchange NMR), but completed by modulated DSC (MDSC),[64] by ordinary DSC (measured in our laboratory), and by photon correlation spectroscopy (PCS).[65] The last method gives both α and β signals.

To deduce a typical frequency ω from a cooling or heating rate, $\dot{T}$, for DSC, we used the equation[16,17]

$$\omega = \frac{\dot{T}}{\delta T}\, a \tag{3.5}$$

with δT the temperature fluctuation of the α functional subsystem, and a a constant. The δT value can be estimated from the ΔT width of the heating-run c_p step.[19] From a comparison of DSC with heat capacity spectroscopy (HCS) for several polymers, a mean value of log $a = -1 \pm 1$ was obtained.[66] Using this a value, we obtained the DSC symbols in Figure 8. The large log a uncertainty does not influence our conclusion below. Direct measurement of PnBMA by HCS is now under way.

We conclude from Figure 8 that the α frequency difference between the G'' peak and NMR frequencies on the one hand and all the other signals on the other hand is even larger (up to 3 decades) at the smaller cooperativity ($\xi_\alpha = 1.1$ nm at $T_g = 26$ °C; see Table 3) than for the larger T_g cooperativity in the PVAC, PS, and NR samples of Table 5. The difference between the shear loss modulus and the dielectric loss function at $T = 22$ °C is clearly demonstrated as an example in Figure 9 (1000 K/$T = 3.39$). The G'' curve only shows a broader low-frequency flank, whereas the ϵ'' curve has two clearly separated maxima. The underlying α and β peaks for ϵ'' are more separated than for G''.

For the local β relaxation no significant difference of the peak frequencies for different activities can be observed, as expected from polyethylene results.[67] Interpreting these facts on the basis of a dispersion law in the $\alpha\beta$ splitting region, we find that the G'' peak and exchange NMR times (for α) correspond to rather short mode lengths of the cooperative α process, smaller than 1 nm, but perhaps somewhat larger than the typical lengths for the local β process (perhaps 0.5 nm, or even smaller).

E. The Additional Shoulder in Polyisobutylene (PIB). It has been known for a long time that the shear loss factor of polyisobutylene (PIB), tan δ, has a clear shoulder on the high-frequency side.[68−71] We try to enlarge the knowledge by inclusion of heat capacity spectroscopy data and dielectric function for bromobutyl rubber (BIIR). Opposite to the case of PIB this polymer has a considerable polarization and allows precise dielectric investigations of the α relaxation.

The whole set of shear master curves for PIB is shown in Figure 10. Both the relaxation (H) and the retarda-

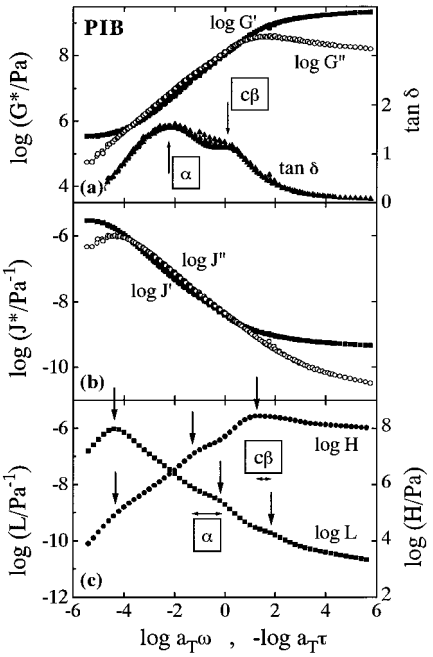

Figure 10. Master plot of (a) shear modulus, G^*, and mechanical loss tangent, tan δ, (b) shear compliance, J^*, and (c) retardation spectrum, L, and relaxation spectrum, H, for polyisobutylene. The reference temperature is −58.9 °C. The main peaks and two shoulders in L and H are indicated by arrows. The two glass transitions are labeled by $\alpha_1 \equiv c\beta$ and $\alpha_2 \equiv \alpha$ (see text).

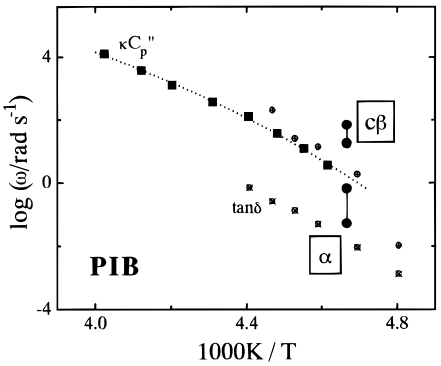

Figure 11. Temperature dependence of the main transition for polyisobutylene. The traces for the main peak of the entropy compliance, $\kappa C_p''$ (■), and for the peak and shoulder of the mechanical loss tangent, tan δ (⊗,⊕), are shown. The full circles (●) in the two dumbbells map the arrows of α and $c\beta$ relaxation in the H and L spectra (see Figure 10). The dotted line is a WLF fit to the $\kappa C_p''$ data.

tion (L) spectrum show, apart from the main peaks, *two* additional slight shoulders, in contrast to the usually found single shoulder in "ordinary" polymers.[4,42] So we have three relaxation zones that are indicated by peaks or shoulders: the hindering zone (HZ) and "two glass transitions", labeled here by $\alpha_1 \equiv c\beta$ and $\alpha_2 \equiv \alpha$. One question is whether a proper glass transition can be identified with α_1 or α_2 in the sense as defined in the Introduction.

The trace of the frequency for the real part $C_p'(\omega,T)$ at half step height (corresponding to the C_p'' maximum) in the Arrhenius diagram is shown in Figure 11. It can be compared (for T_{ref} = −58.9 °C, 1000 K/T_{ref} = 4.67) with the master curve labels for the H and L peaks/shoulders of Figure 10: The two dumbbells of Figure 11 correspond to the arrow pairs of Figure 10c for $\alpha_1 \equiv c\beta$ and $\alpha_2 \equiv \alpha$. It is the α relaxation that is closer to

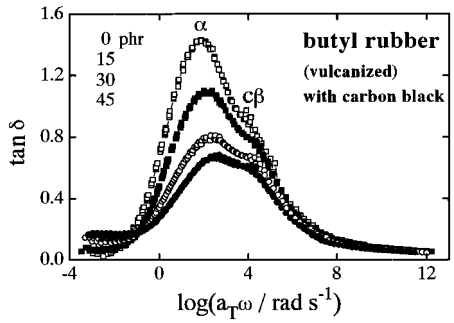

Figure 12. Master curves of shear loss tangent, tan δ, for cross-linked butyl rubbers with different carbon black content ((□) 0 phr; (■) 15 phr; (○) 30 phr; (●) 45 phr). The reference temperature is −20.8 °C.

the heat capacity trace, but a clear decision cannot be reached.

The two tan δ labels of Figure 10a are also transferred to this Arrhenius diagram. As is well known, the tan δ peaks are shifted to lower frequencies when compared to the G'' peak. The C_p' trace can, therefore, not directly be compared with the tan δ values or traces. The temperature dependence of the two tan δ traces indicates encroachment to lower temperatures.

A further argument is expected from a comparison with carbon black filled rubbers. It is well known that carbon black reduces the shear loss factor tan δ of the glass transition of rubbers to a large degree. The influence of carbon black on tan δ for PIB is shown in Figure 12. It is the α peak that is heavily depressed by the carbon black, whereas the $c\beta$ shoulder is hardly, if any, influenced by the filler. We expect that it is the large modes that are (first) influenced by the filler. Therefore, we conclude that the $c\beta$ relaxation is of smaller size than the α relaxation.

A possible interpretation of the $c\beta$ relaxation is given in the paper of Martin and Gillham.[71] They showed in a series of polyolefins of the $[-(CH_2)_m-C(Me)_2-]_n$ structure that the secondary β relaxation, well separated from α for $m = 3$ and $m = 2$, merges completely with α for $m = 1$, i.e. for PIB. We call therefore the $\alpha_1 \equiv c\beta$ relaxation the "captured β relaxation". From the Arrhenius diagram Figure 11 we see that $c\beta$ has a large slope, which means that it is no longer a local process (with a straight line in the Arrhenius diagram). For this reason the $c\beta$ could also be named the "cooperative β relaxation". The encroachment can be interpreted in the spirit of ref 16. Using the terms of the latter reference, the α is the "long" (large scale) and $c\beta$ the "short" (small scale) glass transition, because $T_{\infty\alpha} < T_{\infty c\beta}$. This also confirms the more local nature of the $c\beta$ relaxation, as expected above from the $m \rightarrow 1$ merging of a local β process and the less influence of the carbon black concentration.

The picture can be completed by investigating the dielectric function of bromobutyl rubber (BIIR). The complete set of the different activities is shown in Figure 13, and the BIIR Arrhenius diagram is plotted in Figure 14. The relative C_p'' position of BIIR is not changed in comparison to PIB: The C_p'' maximum (and the corresponding length label assumed to be 3 nm) are between $\alpha_1 \equiv c\beta$ and $\alpha_2 \equiv \alpha$ relaxations as defined by shear. The main peak of dielectric loss (ϵ'') is close by, but significantly different from, the C_p'' peak, similar to the other polymer examples in section 3C. But the shoulder in ϵ'' is on the left (low frequency) flank. This means that a part of the hindering zone (right flank of the L peak)

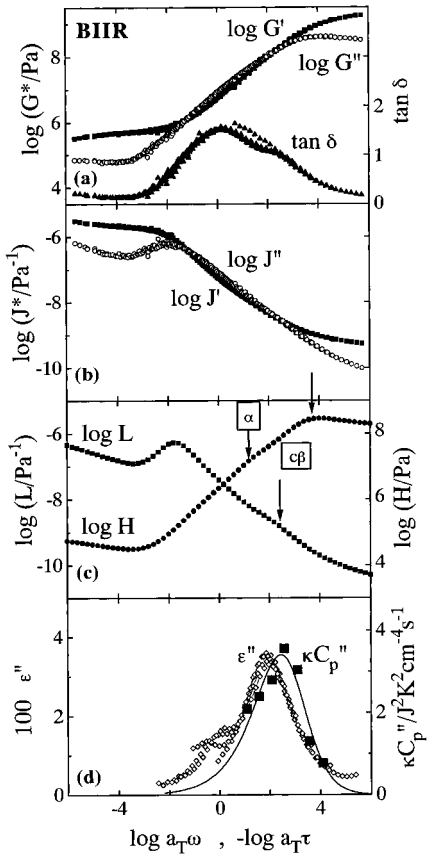

Figure 13. Master plot of (a) shear modulus, G^*, and mechanical loss tangent, tan δ, (b) shear compliance, J^*, (c) retardation spectrum, L, and relaxation spectrum, H, and (d) dielectric loss ϵ'' for bromobutyl rubber (BIIR). Additionally, the loss part of the entropy compliance $\kappa C_p''$ (■) is shown in (d). The solid $\kappa C_p''$ line comes from a HN fit for the corresponding real part $\kappa C_p'$. The reference temperature is always −41.3 °C. The main peaks and shoulders in L and H are indicated by arrows. The two glass transitions are labeled by $\alpha_1 \equiv c\beta$ and $\alpha_2 \equiv \alpha$ (see text).

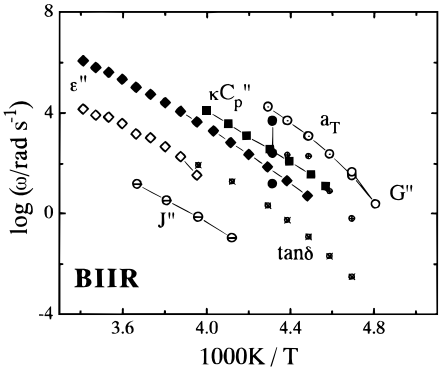

Figure 14. Temperature dependence of different activities in the main transition of bromobutyl rubber (BIIR). The traces for the peak and shoulder of the dielectric loss factor, ϵ'' (♦,◇), and of the mechanical loss tangent, tan δ (⊗,⊕), are shown. The main peak positions of the entropy compliance, $\kappa C_p''$ (■), of the shear compliance, J'' (⊖), and of the shear loss modulus, G″ (○), are also presented. Additionally, the shift factors, a_T (⊙), from the master curve construction for G^* are given. The full circles (●) map the arrows of α (single point) and $c\beta$ (dumbbell) relaxation in the H and L spectra (see Figure 13). The solid lines are only guides for the eye.

also contributes to the dielectric polarization. There are modes probably larger than 3 nm, although there is no large dipole moment component along the chain.

BIIR is an illustrative example for the possible complexity of, and for different activities in, the main transition of polymers, which obviously goes beyond the suggested picture of only two dispersion components of a fine structure and a confined flow between them.

IV. Conclusion

The examples discussed in this paper show that a rather consistent description of the main transition of many amorphous polymers is possible by using the following terms: Fine structure with usually three components (proper glass transition, confined flow zone, hindering zone), the characteristic length of the proper glass transition (ξ_α) of order 3 nm, the entanglement spacing (d_E) of order 7 nm, dispersion law(s) scaling the larger lengths λ with the larger relaxation times τ across the main transition, and the concept of short and long glass transitions[16] explaining the encroachment by eq 1.6, i.e. that the long glass transition (here the hindering zone) has a lower Vogel temperature than the short glass transition (here the proper glass transition).

The main open questions are the existence of a common dispersion law $\tau(\lambda)$ for the different activities, and the value of its exponent, d log τ/d log λ (=2 for hydrodynamic, =4 for Rouse, and ≈6 for the normal mode relaxation as with eq 3.2), especially its dependence on the polymer type, and a possible correlation to the shear exponent in the main transition, d log G'/d log ω = 0.7−1.5 (see Table 5). It seems to be obvious that the local viscosity or the friction coefficient governing the middle part of the main transition of polymers is small when compared to the zero shear rate viscosity η_0 and that the local viscosity is generated by the proper glass transition, not by disentanglement.

The following is a speculative description of possible events occurring when the main transition is crossed starting from short times (high frequencies) in the glassy zone: The main transition is prepared by an Andrade mechanism (shear compliance $J(t)$ exponents between 0.2 and 0.4)[74−77] in the glassy zone, unknown in molecular detail and consisting perhaps of a successive (sequential) combination of more and more (local) β relaxations.[78,79] Then the cooperative proper glass transition (PGT) comes into play at a glass time τ_g. This transition is a cooperative molecular motion with a cooperativity degree of order 100 monomeric units from different polymer chains going through a Cartesian volume of $\xi_\alpha^3 \approx 30$ nm^3. The monomeric units reach a mobility that allows them to flow with a rather low shear viscosity of order $G_g\tau_g$. Thus, in the middle part of the main transition, at length scales between ξ_α and d_E, we find some kind of confined flow (CF) that, perhaps, undermines (or hides?) the Rouse modes. It would be important to obtain independent information about a dispersion law (general scaling law) in this flow zone. This flow is probably more or less modified by the chain structure linking the monomeric units, and for larger lengths, it is certainly hindered and finally confined by the entanglements. This hindering zone (HZ) should also be considered to be some kind of a "long" glass transition with larger cooperativity elements than the monomeric units. This is indicated by an independent WLF equation for it.[2,18,30] Beyond the hindering zone, in the rubbery plateau zone, the next, the terminal or flow transition, is prepared by a second Andrade process.

We propose chain parts as the "particles" of the long glass transition (HZ) since the deformation of a chain

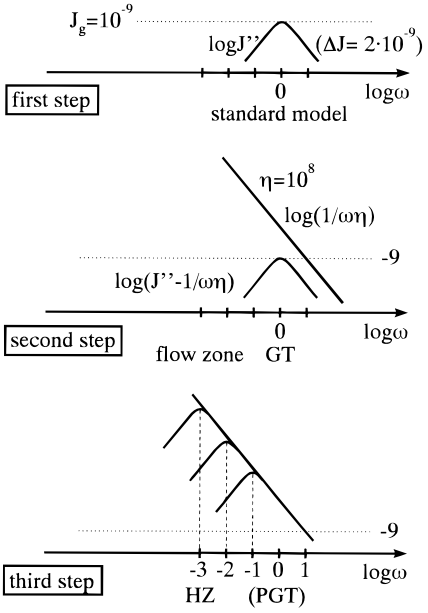

Figure 15. Three-step model for confined flow (explanation in the main text).

coil is monitored by thermal energy of order kT only. So this long glass transition can also be dominated by fluctuations.

In the following, we suggest an intuitive picture for the explanation of the low viscosity of confined flow: Assuming that the chain parts can more easily move in chain direction than transverse, the confined flow consists of *longitudinal* and therefore low-viscosity motions of individual chain parts. We would then have a "fluctuating tube" of "fluctuating length" for any chain part with a tube diameter of about 0.5 nm, so to speak some kind of small-scale reptation of chain parts between the entanglements. Using this picture, the entanglement spacing d_E is that length scale where the longitudinal low-viscosity flow of individual chain parts is modified by the fact that the longer chain parts, due to the chain coiling curvature assisted by tube fluctuation, get necessarily transversal components, which are, of course, more hindered than the longitudinal one.

Lowering the temperature (preventing aging effects by means of eternal equilibration times) increases[18] the characteristic length ξ_α, whereas the entanglement spacing remains nearly constant. This means that the confined flow zone is narrowed by the encroachment not only relative to the time but also relative to the length scale, and finally the confined flow dissolves itself at the crossing of the WLF curves for proper glass transition and hindering zone.

Raising the temperature decreases the characteristic length. Obviously, remarkable enough, this seems to diminish the possibility of confined flow so that Rouse modes become dominant in the splitting region (small or no cooperativity) and beyond. There is no contradiction to the intuitive longitudinal character of confined flow for individual chain parts, since the Rouse modes as well include all three space dimensions, thus including the locally longitudinal one.

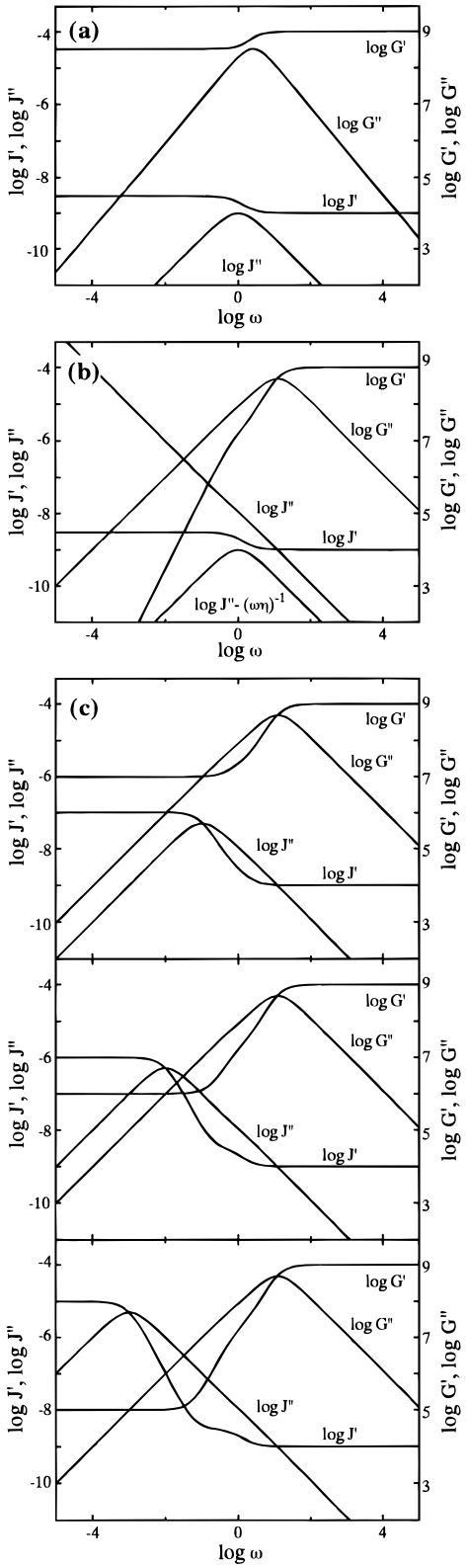

Figure 16. Viscoelastic properties of the three steps of the model of Figure 15. The third step shows some similarity with Figure 1, including Plazek's slight shoulder at the proper glass transition.

Acknowledgment. The authors are grateful to Prof. C. Schick (Universität Rostock) for support during the MDSC measurements and stimulating discussions. The help of Dr. A. Schönhals (Zentrum für Angewandte Chemie Berlin-Adlershof) in carrying out the dielectric measurements on different poly(alkyl methacrylate)s is acknowledged. The authors also thank Dr. J. Lange (Universität Halle) for his help and assistance with the PCS measurements. E.D. thanks Dr. K. L. Ngai for an intensive discussion of a first version of this paper. This work was partly supported by the Deutsche Forschungsgemeinschaft (DFG), the Bundesministerium

für Bildung und Forschung (BMBF), the Fonds der Chemischen Industrie, and the Land Sachsen-Anhalt.

Appendix. Compliance Model for Confined Flow

This section presents a simple, constructive three-step model to illustrate what is meant by the term confined flow. In the first step, a simple Lorentz line for compliance $J^*(\omega)$ is considered, with the parameters log $\omega_{max} = 0$ and $\Delta J = 2 \times 10^{-9}$ (Pa^{-1}), based on a glass compliance $J_g = 1 \times 10^{-9}$ (standard model). In the second step, a viscosity term $J'' = 1/\omega\eta$ is added with $\eta = 10^{+8}$, corresponding to a flow zone generated by the glass transition (GT) corresponding to step one. The third step consists of two dispersions: the proper glass transition (PGT) corresponding to the Lorentz line of step one (now indicated by the symbol PGT in the lower part of Figure 15), plus a second dispersion zone (hindering zone, HZ). The latter is a Lorentz line at lower frequency with a high-frequency flank in J'' exactly corresponding to the viscosity term of the second step. The confined flow is therefore modeled by the fixed right flank of the hindering zone. Three variants of the third step are modeled with HZ maxima for J'' at log $\omega = -1$, -2, and -3.

The dynamic shear curves for all three model steps are shown in Figure 16. The first step corresponds to a solid-state standard relaxation. The second step corresponds to a dynamic glass transition of small-molecule glass formers having a steady-state compliance J_e^0 different from J_g (see e.g. ref 72). The third step corresponds to the main transition in polymers with a three-component fine structure: The proper glass transition PGT at log $\omega = 0$ (Plazek's slight shoulder[42] is also indicated in an exaggerated shape), the confined flow (CF) zone, and the hindering zone (HZ) at the log ω values indicated in Figure 15. The confined flow is generated by the proper glass transition and is formally modeled by the constant right hand side flank of the HZ. The rubbery plateau value is adjusted by the maximum frequency of the hindering zone (-1, -2, and -3 in the third step). The terminal flow transition at low frequency log $\omega < 3$ is not modeled; the corresponding polymer viscosity is much higher than the confined flow viscosity η.

Figure 16 shows that a satisfactory agreement with the overall picture for both glass transitions in small-molecule substances[72] and polymers (Figure 1) can be achieved with this simple three-step model. The steepest shear exponent for the bottom diagram is about 1.5. This model is an indication that J_e^0 values of the proper glass transition can be determined from Plazek's slight shoulder.[73] Observe that all curves of Figure 16 are only modeled by two Lorentz lines and one selected viscosity, so that there is no hope to model the many components of the more complex PIB or BIIR spectra with it.

References and Notes

(1) Ferry, J. D. *Viscoelastic Properties of Polymers*; Wiley: New York, 1980.
(2) Ngai, K. L.; Plazek, D. J. *Rubber Chem. Technol.* **1995**, *68*, 376.
(3) Donth, E.; Schneider, K. *Acta Polym.* **1985**, *36*, 273, 213.
(4) Reissig, S.; Beiner, M.; Vieweg, S.; Schröter, K.; Donth, E. *Macromolecules* **1996**, *29*, 3996.
(5) Sillescu, H. *Acta Polym.* **1994**, *45*, 2; and preprint.
(6) Stannarius, R.; Kremer, F.; Arndt, M. *Phys. Rev. Lett.* **1995**, *75*, 4698.
(7) Ediger, M. D.; Angell, C. A.; Nagel, S. R. *J. Phys. Chem.*, to be published.
(8) Sillescu, H. *Phys. Rev. E* **1996**, *53*, 2992.
(9) Stillinger, F. H.; Hodgdon, J. A. *Phys. Rev. E* **1996**, *53*, 2995.
(10) Katana, G.; Fischer, E. W.; Hack, Th.; Abetz, V.; Kremer, F. *Macromolecules* **1995**, *28*, 2714.
(11) Kumar, S. K.; Anastasidis, S. H.; Fytas, G. *Concentration Fluctuation Induced Dynamic Heterogeneities in Polymer Blends and Block Copolymers*, preprint.
(12) Cicerone, M. T.; Blackburn, F. R.; Ediger, M. D. *Macromolecules* **1995**, *28*, 8224.
(13) Ediger, M. D.; Inoue, T.; Cicerone, M. T.; Blackburn, F. R. *Macromol. Symp.* **1996**, *101*, 139.
(14) Holzer, B.; Strobl, G. *Acta Polym.* **1996**, *47*, 40.
(15) Liu, C. Z. W.; Oppenheim, I. *Phys. Rev. E* **1996**, *53*, 799.
(16) Donth, E. *Relaxation and Thermodynamics in Polymers. Glass Transition*; Akademie-Verlag: Berlin, 1992.
(17) Donth, E. *Glasübergang*; Akademie-Verlag: Berlin, 1981.
(18) Donth, E. *J. Non-Cryst. Solids* **1982**, *53*, 325.
(19) Schneider, K.; Schönhals, A.; Donth, E. *Acta Polym.* **1981**, *32*, 471.
(20) Plazek, D. J. *Polym. J.* **1980**, *12*, 43.
(21) Donth, E.; Michler, G. H. *Colloid Polym. Sci.* **1989**, *267*, 557.
(22) Rouse, P. E. *J. Chem. Phys.* **1953**, *21*, 1272.
(23) Richter, D.; Ewen, B.; Farago, B.; Wagner, T. *Phys. Rev. Lett.* **1989**, *62*, 2140.
(24) Higgins, J. S.; Nicholson, L. K.; Hayter, J. D. *Polymer* **1981**, *22*, 163.
(25) Vorst, B. van der; Toose, E. M.; Ende, D. van den; Jongschaap, R. J. J.; Mellema, J. *Rheol. Acta* **1995**, *34*, 274.
(26) Slater, G. W.; Wu, S. Y. *Phys. Rev. Lett.* **1995**, *75*, 164.
(27) Richter, D.; Willner, L.; Zirkel, A.; Farago, B.; Fetters, L. J.; Huang, J. S. *Phys. Rev. Lett.* **1993**, *71*, 4158.
(28) Greassley, W. W. *Adv. Polym. Sci.* **1982**, *47*, 67.
(29) Williams, M. L.; Landel, R. F.; Ferry, J. D. *J. Am. Chem. Soc.* **1955**, *77*, 3701.
(30) Pfandl, W.; Link, G.; Schwarzl, F. R. *Rheol. Acta* **1984**, *23*, 277.
(31) Ferry, J. D.; Fitzgerald, E. R. *J. Colloid Sci.* **1953**, *8*, 224.
(32) Ferry, J. D.; Strella, S. *J. Colloid Sci.* **1958**, *13*, 459.
(33) Donth, E.; Schenk, W.; Ebert, A. *Acta Polym.* **1979**, *30*, 540.
(34) Colmenero, J.; Alegria, A.; Alberdi, J. M.; Alvarez, F.; Frick, B. *Phys. Rev. B* **1991**, *44*, 7321.
(35) Böhmer, R.; Sanchez, E.; Angell, C. A. *J. Phys. Chem.* **1992**, *96*, 9089.
(36) Colmenero, J.; Alegria, A.; Santangelo, P. G.; Ngai, K. L.; Roland, C. M. *Macromolecules* **1994**, *27*, 407.
(37) Roland, C. M. *Macromolecules* **1995**, *28*, 3463.
(38) Beiner, M.; Korus, J.; Lockwenz, H.; Schröter, K.; Donth, E. *Macromolecules* **1996**, *29*, 5183.
(39) Beiner, M. Thesis; Universität Halle, 1995.
(40) Garwe, F.; Schönhals, A.; Lockwenz, H.; Beiner, M.; Schröter, K.; Donth, E. *Macromolecules* **1996**, *29*, 247.
(41) Giebel, L.; Meier, G.; Fytas, G.; Fischer, E. W. *J. Polym. Sci., B: Polym. Phys.* **1992,** *30*, 1291.
(42) Reissig, S.; Beiner, M.; Korus, J.; Schröter, K.; Donth, E. *Macromolecules* **1995**, *28*, 5394.
(43) Birge, N. O.; Nagel, S. R. *Phys. Rev. Lett.* **1985**, *54*, 2674.
(44) Bierbach, T. Diploma thesis, Universität Halle, 1995.
(45) Beiner, M.; Garwe, F.; Hempel, E.; Schawe, J.; Schröter, K.; Schönhals, A.; Donth, E. *Physica A* **1993**, *201*, 72.
(46) Lomellini, P.; Lavagnini, L. *Rheol. Acta* **1992,** *31*, 175.
(47) Honerkamp, J.; Weese, J. *Rheol. Acta* **1993**, *32*, 65.
(48) Havriliak, S.; Negami, S. *J. Polym. Sci., Part C: Polym. Symp.* **1966**, *14*, 99.
(49) Schlosser, E.; Schönhals, A.; Carius, H. E.; Goering, H. *Macromolecules* **1993**, *26*, 6027.
(50) Garwe, F.; Beiner, M.; Hempel, E.; Schawe, J.; Schröter, K.; Schönhals, A.; Donth, E. *J. Non-Cryst. Solids* **1994**, *172*, 191.
(51) Beiner, M.; Garwe, F.; Schröter, K.; Donth, E. *Colloid Polym. Sci.* **1994**, *272*, 1439.
(52) Beiner, M.; Hempel, E.; Garwe, F.; Renner, T.; Donth, E., to be published.
(53) Imanishi, Y.; Adachi, K.; Kotaka, T. *J. Chem. Phys.* **1988**, *89*, 7585, 7593.
(54) Stockmayer, W. H. *Pure Appl. Chem.* **1967**, *15*, 539.
(55) Boese, D.; Kremer, F. *Macromolecules* **1990**, *23*, 829.
(56) Kahle, S. Diploma thesis, Universität Halle, 1995.
(57) Kirst, K. U.; Erman, B.; Kremer, F.; Fischer, E. W., preprint.
(58) Simon, G.; Baumann, K.; Gronski, W. *Macromolecules* **1992**, *25*, 3624.
(59) Plazek, D. J. *J. Polym. Sci., Part A-2* **1966**, *4*, 745.
(60) Wu, L.; Dixon, P. K.; Nagel, S. R.; Williams, B. D.; Carini, J. P. *J. Non.-Cryst. Solids* **1991**, *131−133*, 32.
(61) O'Reilly, J. M.; Sedita, J. S. *J. Non-Cryst. Solids* **1991**, *131−133*, 1140.
(62) Garwe, F.; Schönhals, A.; Beiner, M.; Schröter, K.; Donth, E. *J. Phys.: Condens. Matter* **1994**, *6*, 6941.

(63) Domberger, W.; Reichert, D.; Garwe, F.; Schneider, H.; Donth, E. *J. Phys.: Condens. Matter* **1995**, *7*, 7419.
(64) Garwe, F.; Hensel, A. (MDSC measurements for PnBMA), unpublished results.
(65) Garwe, F.; Janich, M.; Wötzel, D. (PCS measurements for PnBMA), unpublished results.
(66) Donth, E.; Korus, J.; Hempel, E.; Beiner, M. Comparison of DSC Heating Rate and HCS Frequency at the Glass Transition. *Thermochim. Acta*, to be published.
(67) Kakizaki, M.; Kakudate, T.; Hideshima, T. *J. Polym. Sci., Polym. Phys. Ed.* **1985**, *23*, 809.
(68) Ferry, J. D.; Grandine, L. D.; Fitzgerald, E. R. *J. Appl. Phys.* **1953**, *24*, 650, 911.
(69) Plazek, D. J.; Chay, I. C.; Ngai, K. L.; Roland, C. M. *Macromolecules* **1995**, *28*, 6432.
(70) Okamoto, H.; Inoue, T.; Osaki, K. *J. Polym. Sci., B: Polym. Phys.* **1995**, *33*, 1409.
(71) Martin, J. R.; Gillham, J. K. *J. Appl. Polym. Sci.* **1972**, *16*, 2091.
(72) Plazek, D. J.; Bero, C. A.; Chay, I. C. *J. Non-Cryst. Solids* **1994**, *172*, 181.
(73) Ngai, K. L.; Plazek, D. J.; Echeverrier, I., to be published.
(74) Andrade, E. N. da C. *Proc. R. Soc. London, A* **1910**, *84*, 11; **1914**, *90*, 329.
(75) Andrade, E. N. da C. *Philos. Mag.* **1962**, *7*, 2003.
(76) Kennedy, A. J. *J. Mech. Phys. Solids* **1953**, *1*, 172.
(77) Schönhals, A.; Donth, E. *Phys. Status Solidi B* **1984**, *124*, 515.
(78) McCrum, N. G. *Polym. Commun.* **1984**, *25*, 2.
(79) Schönhals, A.; Donth, E. *Acta Polym.* **1986**, *37*, 475.

MA951881A